A Qualitative Comparison of ANSYS and OpenFOAM results for Carbon dioxide Plume Transport

S Madsen[1], Z Andleeb[2], H Khawaja[1]*, G Boiger[3], M Moatamedi[4]

1. UiT-The Arctic University of Norway, Tromsø, Norway
2. Abyss Solutions, Pakistan
3. Zurich University of Applied Sciences (ZHAW), Switzerland
4. New York University, London, United Kingdom

ABSTRACT

This research presents Computational Fluid Dynamics (CFD) simulations in ANSYS illustrating emissions of carbon dioxide to the air. The CFD simulations is employed to study plume transport in urban environment, i.e., Breivika port in the city of Tromsø. The case study presents a two-phase model considering specific wind strength and direction in the city of Tromso. Geographical coordinates, temperature, and wind data were obtained from the open sources, such as Google Maps, and Norwegian Meteorological Institute. The result from the simulations indicates a potential outcome with respect to various weather conditions. It was revealed for vessels less than 30 meters chimney height, the higher the wind strength, the lower the plume dispersion, causing the plume to stay closer to the terrain. This brings in a concentrated emission of pollutants closer to the public areas. The terrain in the model is recognizable for the Tromsø port's location. From the CFD results, it is illustrated that onshore wind with high wind strength could affect the environment. The results simulated in OpenFOAM are qualitatively showing the same as visible in ANSYS..

1. INTRODUCTION

1.1. Computational Fluid Dynamics (CFD)

Computational fluid dynamics (CFD) is a science that, with the help of digital computers, produces quantitative predictions of fluid-flow phenomena based on the conservation laws (conservation of mass, momentum, and energy) governing fluid motion [1,2]. CFD has increased in importance and in accuracy; however, its predictions are never completely exact. Because many potential sources of error may be involved, one has to be very careful when interpreting the results produced by CFD techniques [3-5]. The key to various numerical methods is to convert the partial different equations that govern a physical phenomenon into a system of algebraic equations. Different techniques are available for this conversion. CFD is merely a tool for analyzing fluid-flow problems [6-9]. If it is used correctly, it can provide useful information cheaply and quickly. Different kinds of numerical methods are used in CFD, for example, the finite-difference, finite-element, finite volume, spectral method, and spectral element methods [10,11]. They share the common approach that discretizes the Navier-Stokes equations into a system of algebraic equations.

*Corresponding Author: Hassan.a.khawaja@uit.no

CFD stands for computational fluid dynamics which is based on three principles: conservation of momentum, energy, and mass [6]. Conservation of mass is presented in equation and the symbols are shown in Equation 1,

$$\frac{\partial \rho}{\partial t} + \frac{\partial(\rho u)}{\partial x} + \frac{\partial(\rho v)}{\partial y} + \frac{\delta(\rho w)}{\delta z} = 0 \tag{1}$$

where ρ is fluid density, t is time, u is fluid velocity in x-direction, v is fluid velocity in y-direction, and w is fluid velocity in z-direction.

The formula for conservation of momentum is given by the Navier-Stokes equation in x, y and z directions, respectively, as shown in Equations 2, 3 and 4,

$$\frac{\partial(\rho u)}{\partial t} + \nabla * \left(\rho u \vec{U}\right) = -\frac{\partial p}{\partial x} + \frac{\partial \tau_{xx}}{\partial x} + \frac{\partial \tau_{yx}}{\partial y} + \frac{\partial \tau_{zx}}{\partial z} + pfx = 0 \tag{2}$$

$$\frac{\partial(\rho v)}{\partial t} + \nabla * \left(\rho v \vec{U}\right) = -\frac{\partial p}{\partial x} + \frac{\partial \tau_{xy}}{\partial x} + \frac{\partial \tau_{yy}}{\partial y} + \frac{\partial \tau_{zy}}{\partial z} + pfy = 0 \tag{3}$$

$$\frac{\partial(\rho w)}{\partial t} + \nabla * \left(\rho w \vec{U}\right) = -\frac{\partial p}{\partial x} + \frac{\partial \tau_{xz}}{\partial x} + \frac{\partial \tau_{yz}}{\partial y} + \frac{\partial \tau_{zz}}{\partial z} + pfz = 0 \tag{4}$$

where p is pressure, $\vec{U}$ is velocity vector $(ui + vj + wk)$, $\vec{f}$ is a body force vector $(f_x i + f_y i + f_z k)$, and τ is a shear stress tensor described as $\begin{bmatrix} \tau_{xx} & \tau_{xy} & t_{xz} \\ \tau_{yx} & \tau_{yy} & \tau_{yz} \\ \tau_{zx} & t_{zy} & \tau_{zz} \end{bmatrix}$.

1.2. Gaussian Plume Model

The Gaussian plume model is the most common air pollution model [12,13]. It is based on a simple formula that describes the three-dimensional concentration field generated by a point source under stationary meteorological and emission conditions. Gaussian-based dispersion models are widely used to estimate local pollution levels [14,15]. The dispersion of plume which is emitted from a chimney is governed by many factors i.e., wind direction, wind speed, turbulence intensity, local terrain and temperature.

A point source somewhere in the air where a pollutant is released at a constant rate Q (kg/s). The wind is blowing continuously in a direction x (measured in meters from the source) with a speed U (m/s). The plume spreads as it moves in the x direction such that the local concentrations $C(x, y, z)$ (kg/m^3) at any point in space form distributions which have shapes that are "Gaussian" or "normal" in planes normal to the x direction produce a Gaussian Plume Model as given in Figure 1.

The parameters σ_y and σ_z are the standard deviations of these Gaussian distributions, which indicate the spread of the plume in the y and z directions, respectively. They increase with the distance x from the source. The area under the distribution, determined by integration of the functions given above between plus and minus infinity, is equal to unity. Combining these two-dimensional shape distributions by multiplying the functions together gives us the function for the shape of the distribution in three-dimensions (a kind of "hill" of pollutant) [16] as shown in Equation (5),

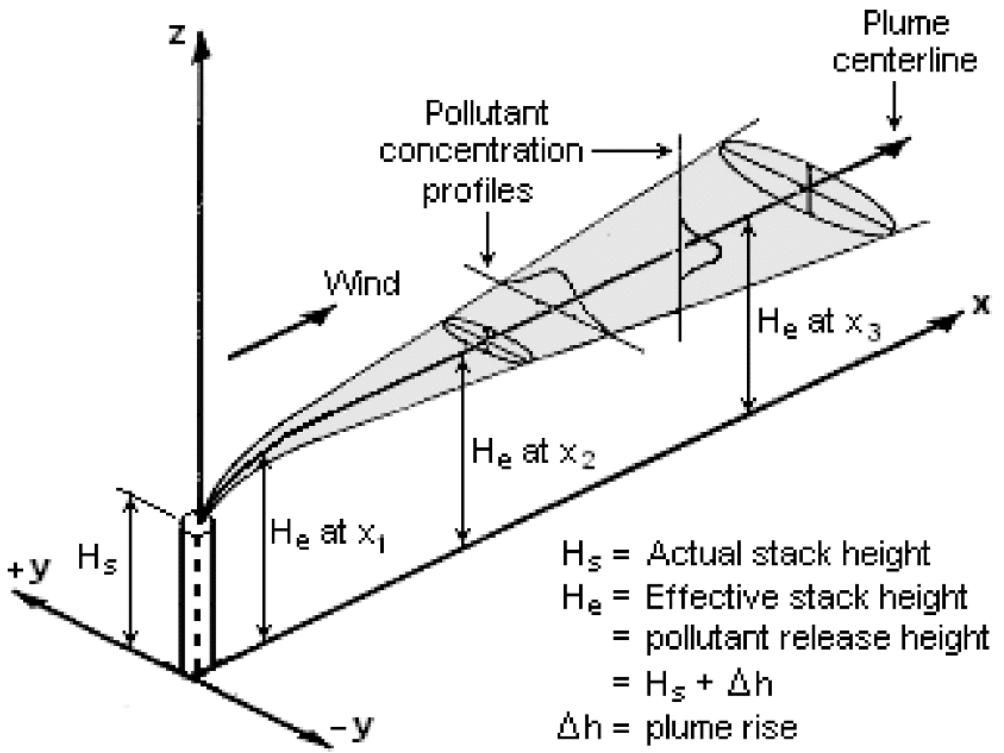

Figure 1. A representation of a Gaussian plume model [11].

$$C(x,y,z) = \frac{Q}{U}\frac{1}{2\pi\sigma_y\sigma_z}\, e^{\left[\frac{-y^2}{2\sigma_y^2}\right]\left[\frac{-(z-H_e)^2}{\sigma_z^2}\right]} \tag{5}$$

where $C(x,y,z)$ is local concentration of plume in the x direction (kg/m^3), Q is pollutant release rate (kg/s), U is speed of wind blowing in x-direction (m/s), σ_y is standard deviation of the Gaussian distribution along the y-axis, σ_y is standard deviation of the Gaussian distribution along the z-axis, H_e is effective height of plume center-line (m) equal to $(H_s + \Delta h)$, H_s is height of source above ground (m), Δh is initial plume rise (m), z is coordinate measured vertically from the ground to a point in the plume (m), and y is coordinate measured along the y-axis to a point in the plume (m).

Hence, the concentration is equal to the rate of emission from the source divided by the wind speed and then multiplied by the shaping function. This distribution measures y and z normally from the x-axis (the x-axis may also be considered to be the direction of the centerline of the plume. In practice, the source will usually be raised above the ground (for example the exit of a chimney). Hence, we need to modify the z coordinate so that it is measured from the ground.

1.3. The Vortex Effect

In fluid dynamics, a vortex is a region in a fluid in which the flow revolves around an axis line, which may be straight or curved. Vortices form in stirred fluids, and may be observed in smoke rings, whirlpools in the wake of a boat, and the winds surrounding a tropical cyclone, tornado or dust devil [17,18].

Vortices are a major component of turbulent flow. The distribution of velocity, vorticity (the curl of the flow velocity), as well as the concept of circulation are used to characterize vortices. In most vortices, the fluid flow velocity is greatest next to its axis and decreases in inverse proportion to the distance from the axis. In the absence of external forces, viscous friction within the fluid tends to organize the flow into a collection of irrotational vortices, possibly superimposed to larger-scale flows, including larger-scale vortices. Once formed, vortices can move, stretch, twist, and interact in complex ways. A moving vortex carries some angular and linear momentum, energy, and mass, with it [19].

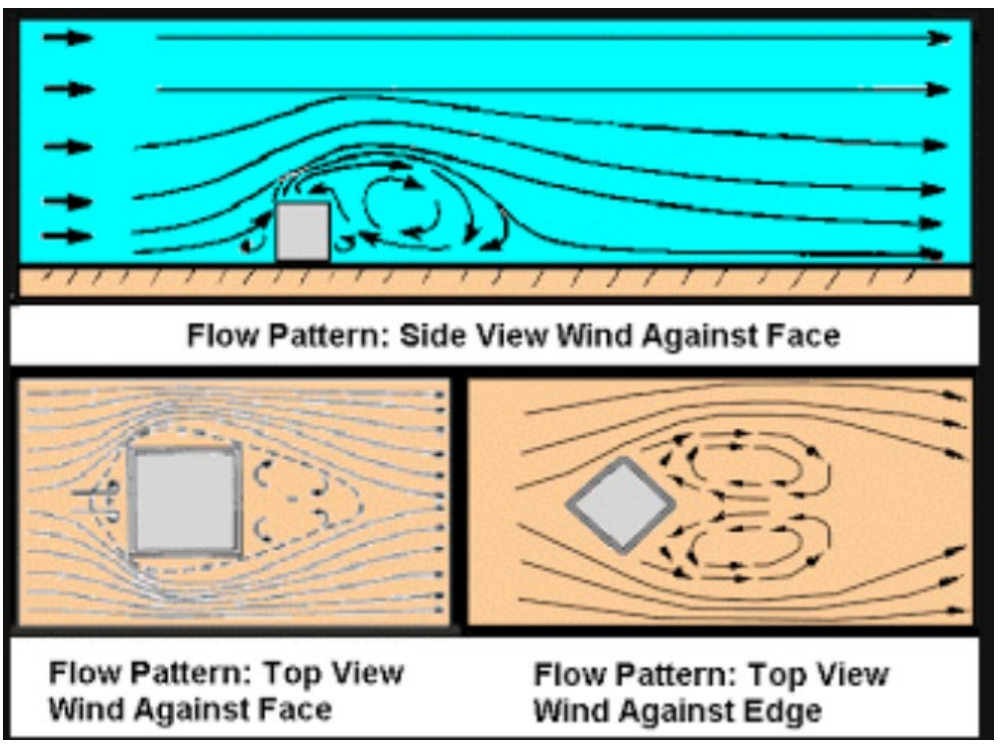

Figure 2: Illustration of the vortex-effect [20].

2. METHODOLOGY

In this study, CFD analysis was performed for four cases of Gaussian carbon dioxide plume models with varying chimney heights in ANSYS as shown in Tables 1. For qualitative comparison, only the critical cases are repeated in OpenFOAM as shown in Table 2.

Table 2. CFD Simulations in ANSYS

chimney height (m)	v_x (m/s)	v_y (m/s)
30	0	15
	0	3.3
	0	1
20	0	15
	0	3.3
10	0	15
	0	3.3
5	0	15
	-5	4.25

Table 2. CFD Simulations in OpenFOAM

chimney height (m)	v_x (m/s)	v_y (m/s)
30	0	5
	-5.4	25

2.1. ANSYS

The ANSYS workbench [21] is used to design the model. The working plane in x, y, and z direction is chosen and the sketching is done. First, a rectangle is created in the wanted dimension where the emission will operate. The construction is a rectangle with a pipe inside, this to simulate a "room" where the gas is released. This box shape allows to have a controlled inlet and outlet of wind, just as a barrier or a wall. One short side represents wind inlet, the second short side represents the wind outlet. The terrain is assumed to be a flat, and the remaining walls are "closed", so the Figure is designed to have a tunnel function.

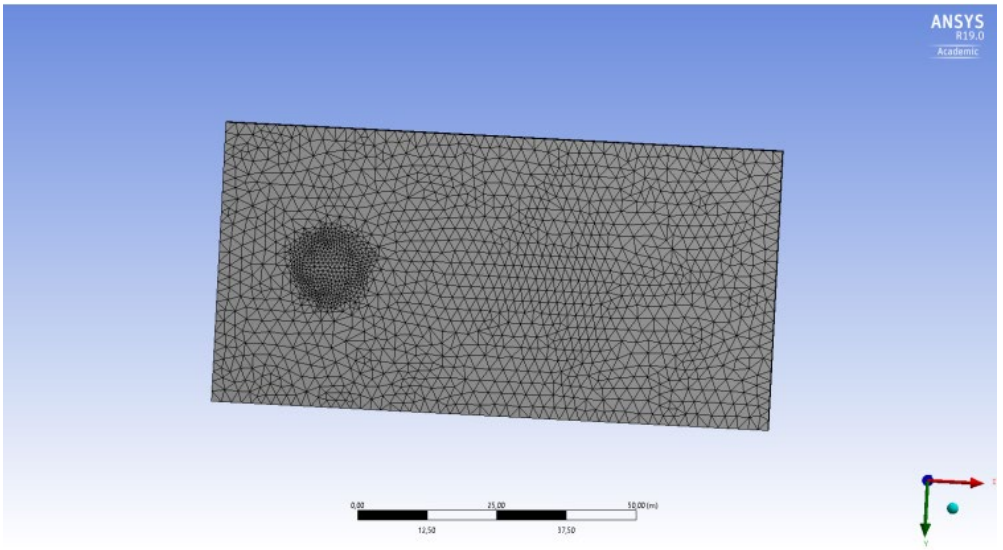

Figure 3: Mesh concentrated to the plume outlet, seen from bottom of Figure.

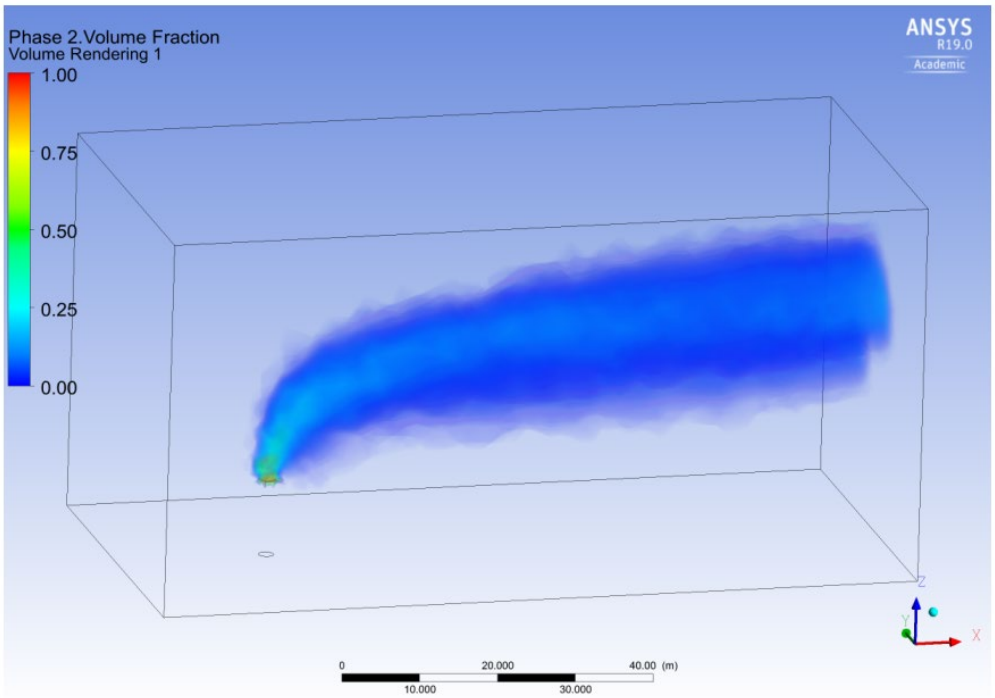

Figure 4: Emission after 60.6 seconds.

The simulation was constructed like a rectangle with a stack inside, to simulate the "room" where the emission is released. The size of the rectangle is 50 meters *100 meters *50 meters, and the pipe inside is centered, so the pipe is located 20 meters away from the short-left hand side. The given dimensions for the pipe are diameter 2 meters, height 5 meters. The diameter of the pipe is set to a realistic measure and have the plume-shape as expected.

To make the simulation as realistic as possible, the most precise location of the simulated area, including existing construction, was used as part of the input data. The programs used for this purpose were Google Earth Pro [22] and TCX Converter [23]. The collection of data points in both distance and height are done using Google Earth Pro. By using the path-function in the software it is possible to collect points with longitude, latitude and altitude, by marking the elements, later called points, which were selected and included in the models shown in Figure 5.

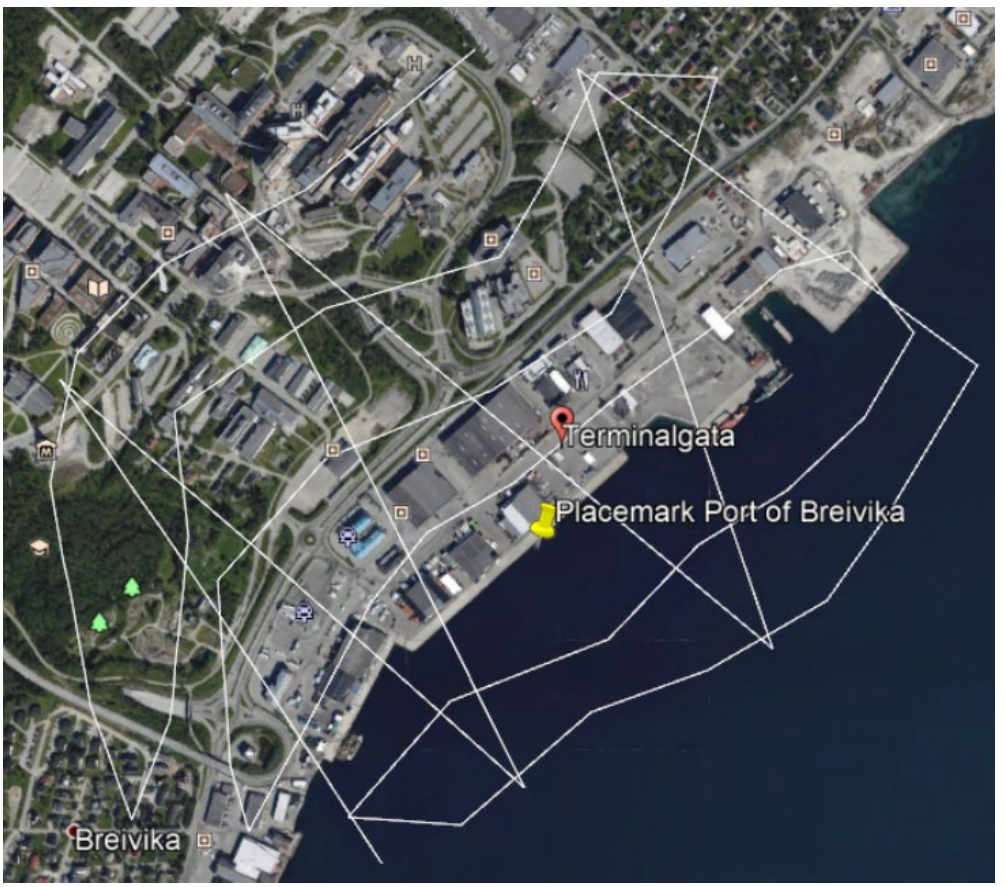

Figure 5: Path containing coordinates near Port of Tromsø, location Breivika

The model is set together of the model file made in SolidWorks and the coordinate file for the buildings. Fluid Flow (Fluent [24]) analysis system is used, and the function Design Modeler was opened. The terrain-file made in SolidWorks was imported as an external geometry file. When the terrain is visible, the function point was indicated and the file with the coordinates of the buildings were imported. The buildings inside the domain for the cylinder were taken into account. To create the buildings, lines were drawn between the different points for the different buildings, generated and thereafter extruded to the wanted height, approximately the height of the buildings as shown in Figures 6 and 7.

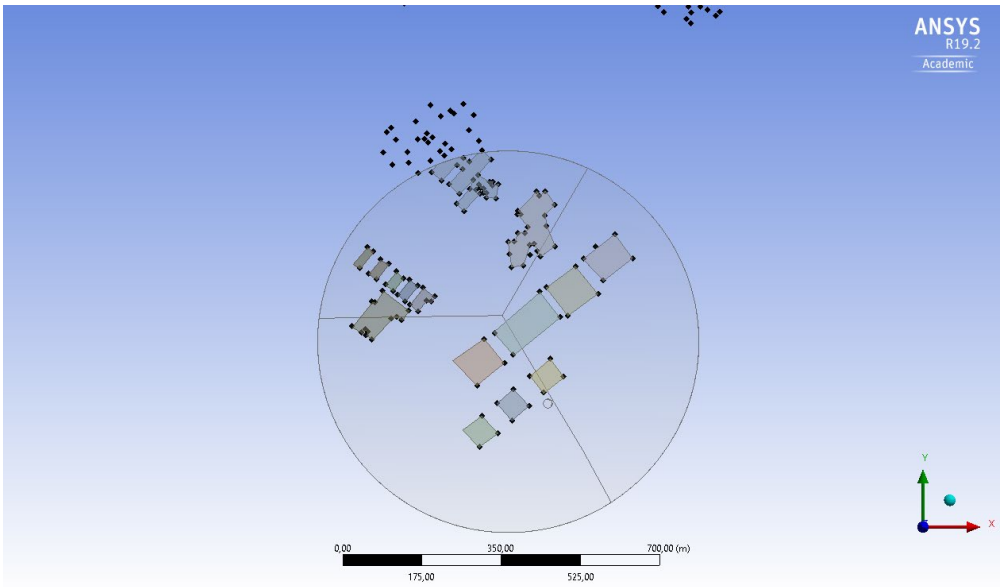

Figure 6: Geometry added to terrain constructed out of geometric points.

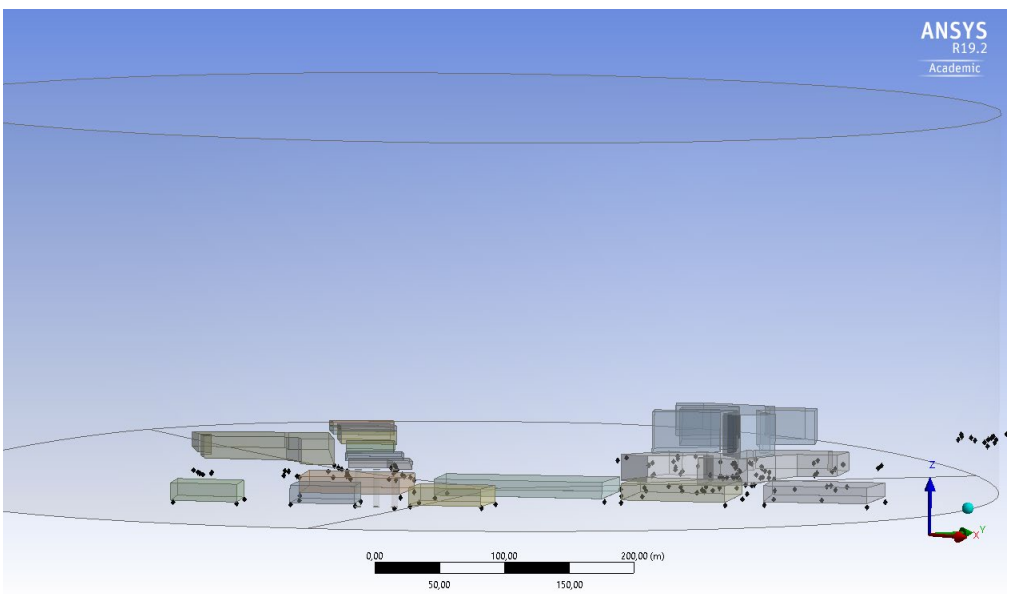

Figure 7: Each building has its own actual height.

Mesh sensitivity analysis was performed to optimize the CFD model. The solution converges at 15 million elements considering the computational power and size of the domain as shown in Figures 8 and 9.

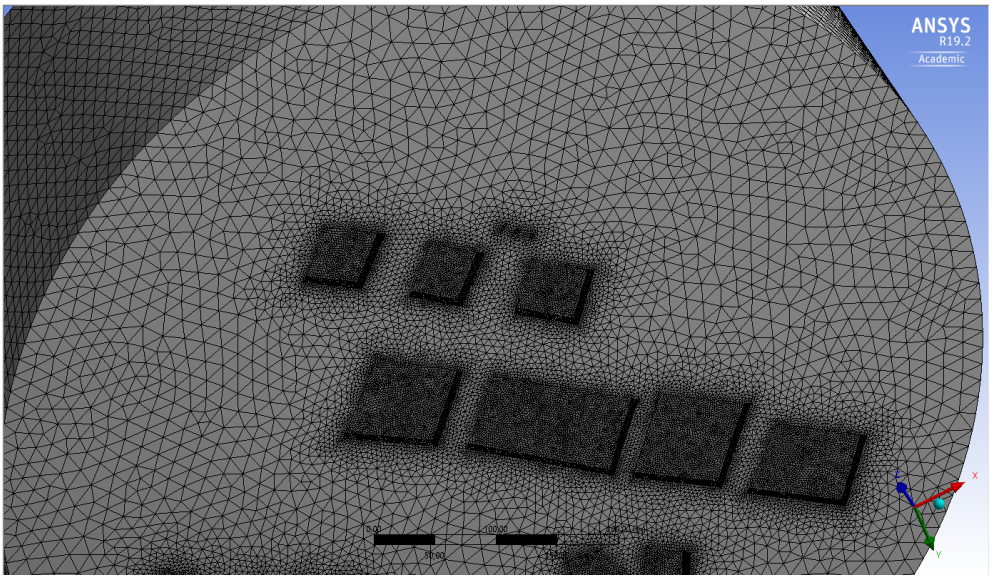

Figure 8: Mesh concentrated around buildings in the terrain.

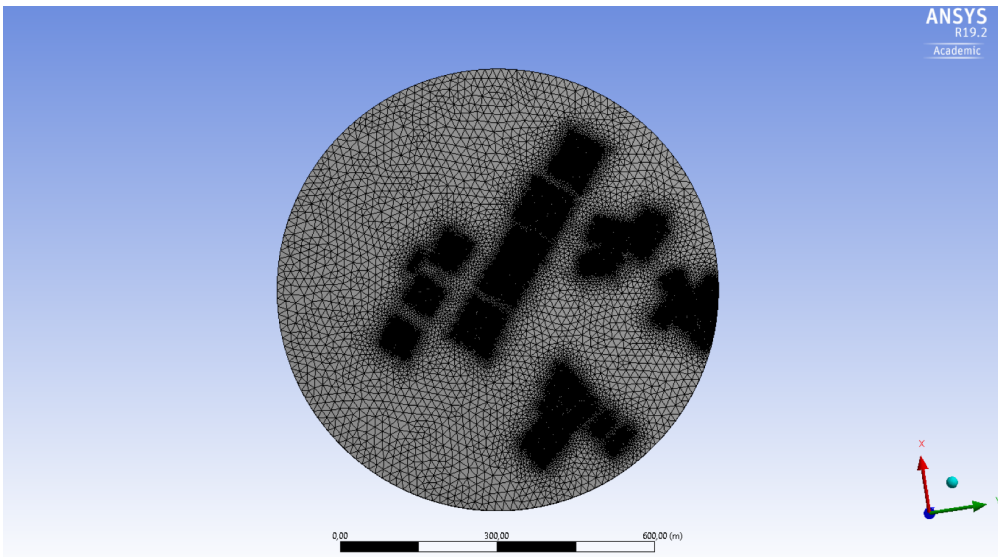

Figure 9: Mesh seen from the bottom.

3. RESULTS AND DISCUSSION

The two-phase model considers wind strength and wind direction, so the result from the simulations indicates a potential outcome if the weather conditions are optimal. CFD simulations were executed to estimate emissions to the air. The highest carbon dioxide content (volume fraction) is colored red, and the smallest amount is colored blue. The OpenFOAM results illustrate the emission dispersion in the same way as ANSYS. It is easy to see the emission flow following the Gaussian Plume model.

From the CFD results, the flow of carbon dioxide near buildings increases when the vessel height decreases, and wind strength increases, as shown in Figure 10. This is because half of the emissions flow against the sea and would disperse before it reaches land.

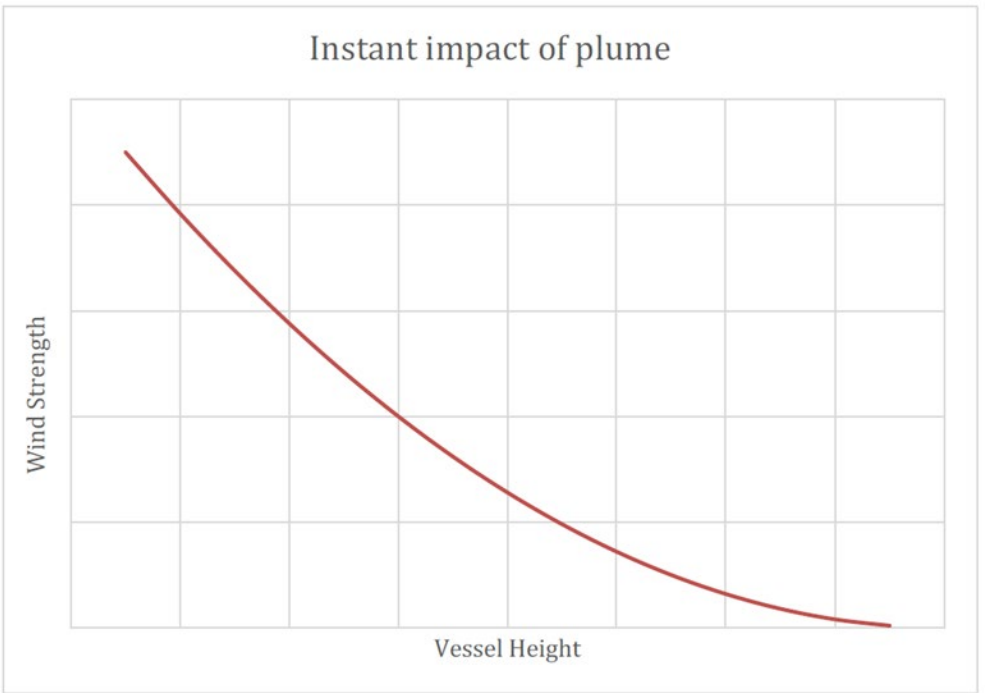

Figure 10: Effect of Wind Strength and Vessel Height on the impact of the plume

With high wind strength, the emission drops faster and will influence closer to the terrain. Low wind strength would make the emission rise above the heights in the landscape and even right up. This could result from emissions of vessels with a height of 30 meters or higher. The emission from a tall vessel might not affect or cause significant pollution in nearby terrain.

The results also illustrate the pollution disperse with low wind strength. The swirling of the pollution is maintained when the strength of the outlet of the pollution decreases. This type of effect can also occur between buildings or when pollution gets trapped, for instance, in a corner of a building. This could result from emissions of vessels with a height of 30 meters or higher. The emission from a tall vessel might not affect or cause significant pollution in nearby terrain. The results also illustrate the pollution disperse with low wind strength. The swirling of the pollution is maintained when the strength of the outlet of the pollution decreases. This type of effect can also occur between buildings or when pollution gets trapped, for instance, in a corner of a building.

3.1. Chimney Height 30m (ANSYS)

The emission profile due to the velocity vector of 15m/s wind condition in y-direction is shown in Figures 11 and 12.

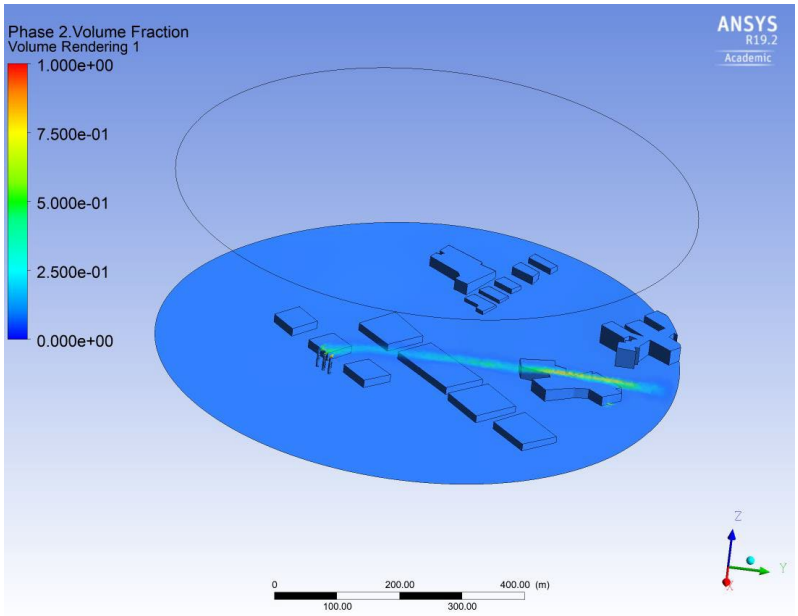

Figure 11: The emission profile under 15 m/s wind conditions (side view).

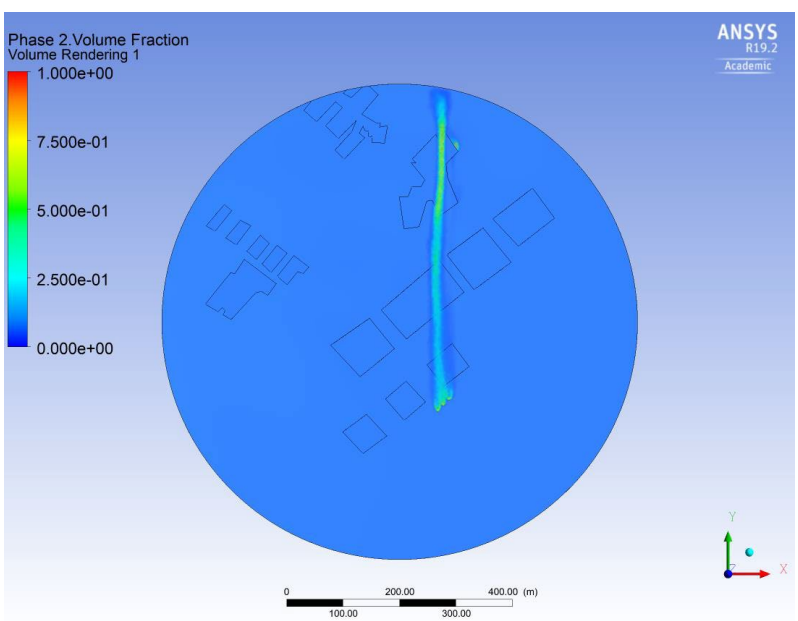

Figure 12: The emission profile under 15 m/s wind conditions (top view).

The emission profile due to the velocity vector of 3.3 m/s wind condition in y-direction is shown in Figures 13 and 14.

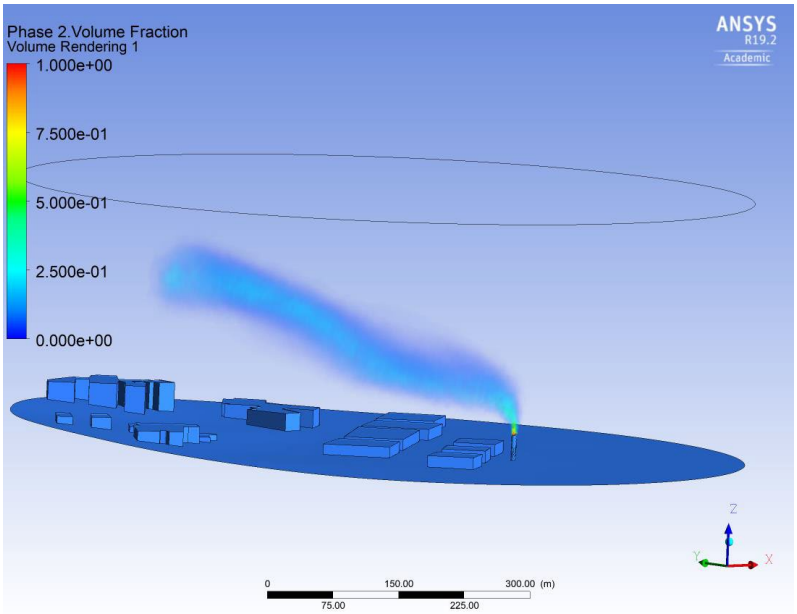

Figure 13: The emission profile under 3.3 m/s wind conditions (side view).

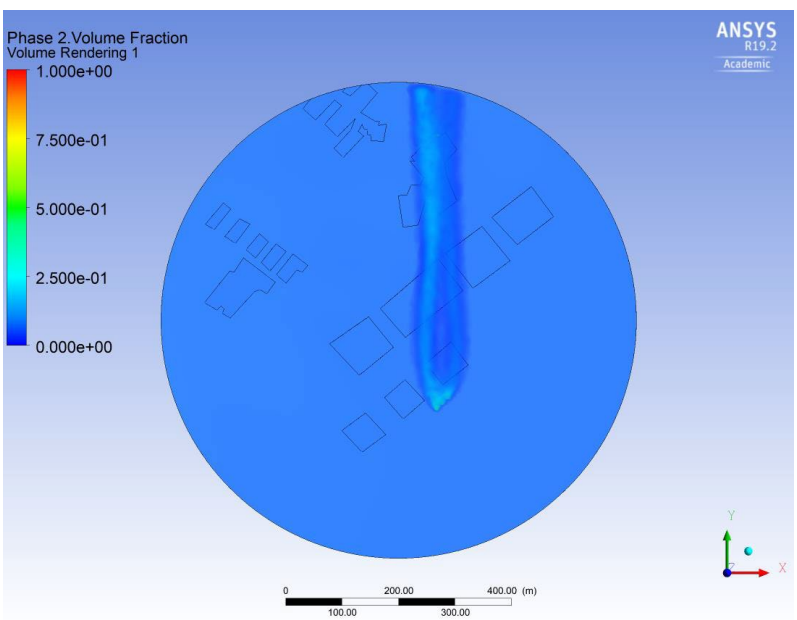

Figure 14: The emission profile under 3.3 m/s wind conditions (top view).

The emission profile due to the velocity vector of 1 m/s wind condition in y-direction is shown in Figures 15 and 16.

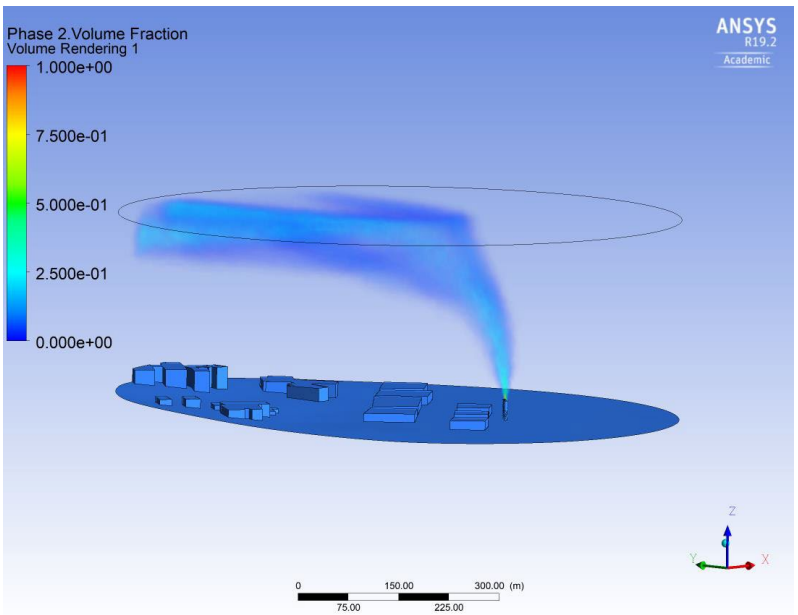

Figure 15: The emission profile under 1 m/s wind conditions (side view).

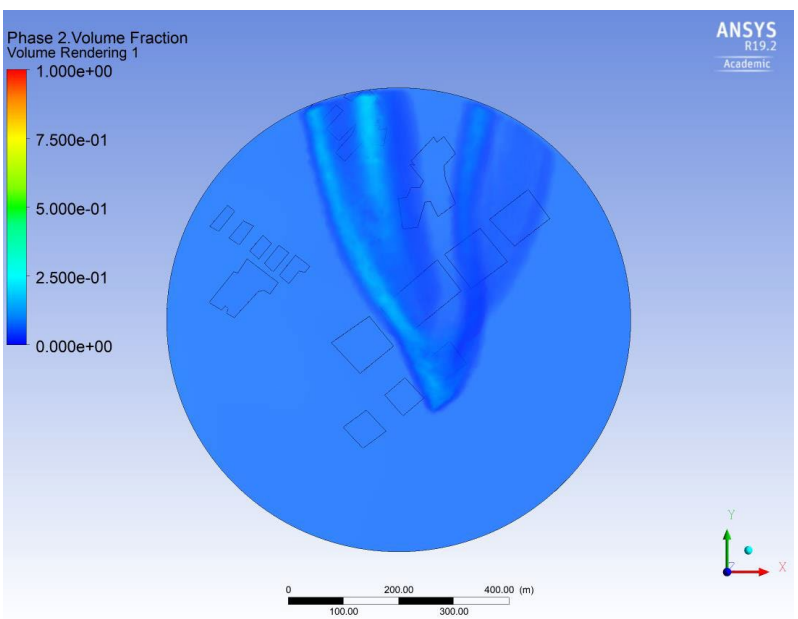

Figure 16: The emission profile under 1 m/s wind conditions (top view).

3.2. Chimney Height 20m (ANSYS)

The emission profile due to the velocity vector of 15 m/s wind condition in y direction is shown in Figures 17 and 18.

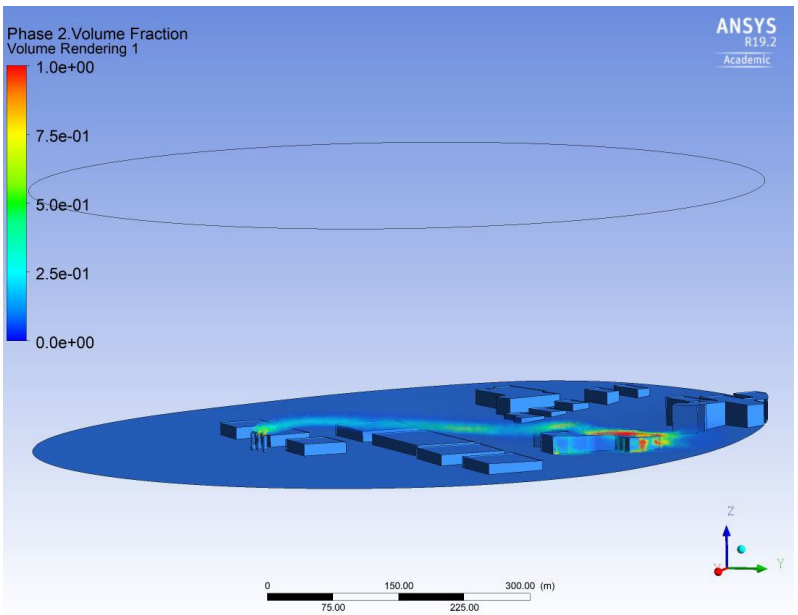

Figure 17: The emission profile under 15 m/s wind conditions (side view).

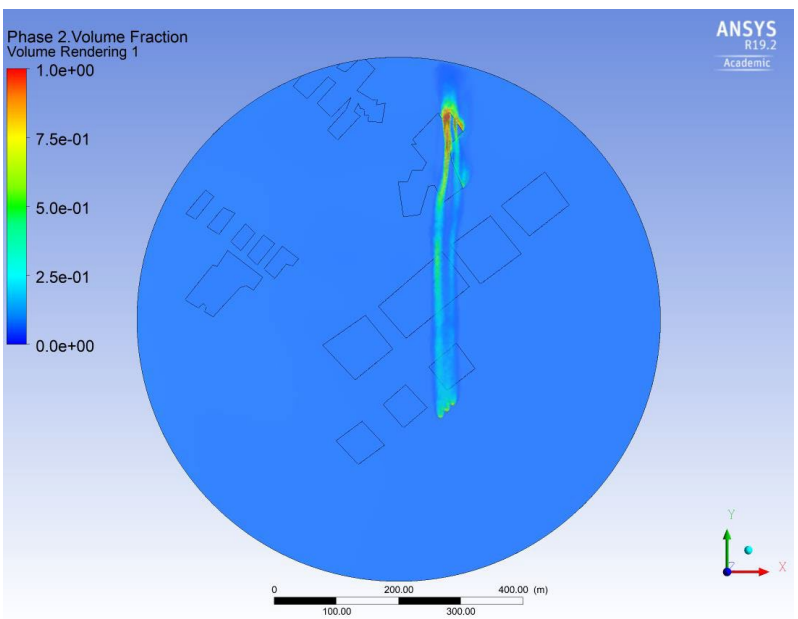

Figure 18: The emission profile under 15 m/s wind conditions (top view).

The emission profile due to the velocity vector of 3.3 m/s wind condition in y directions is shown in Figures 19 and 20.

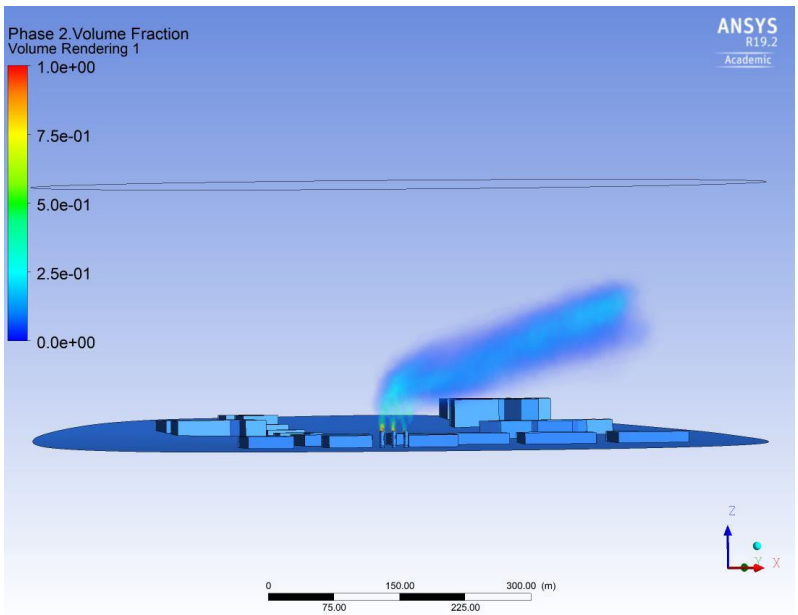

Figure 19: The emission profile under 3.3 m/s wind conditions (side view).

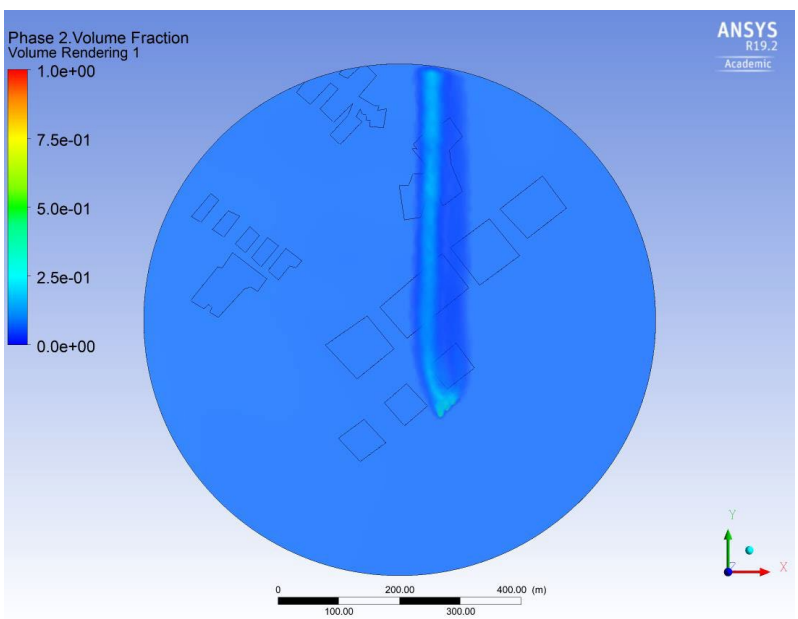

Figure 20: The emission profile under 3.3 m/s wind conditions (top view).

3.3. Chimney Height 10m (ANSYS)

The emission profile due to the velocity vector of 15 m/s wind condition in y direction is shown in Figures 21 and 22.

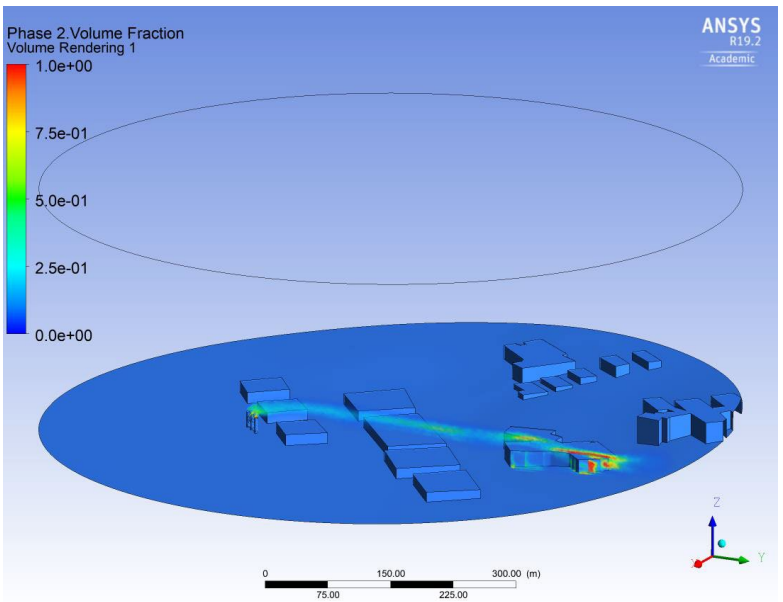

Figure 21: The emission profile under 15 m/s wind conditions (side view).

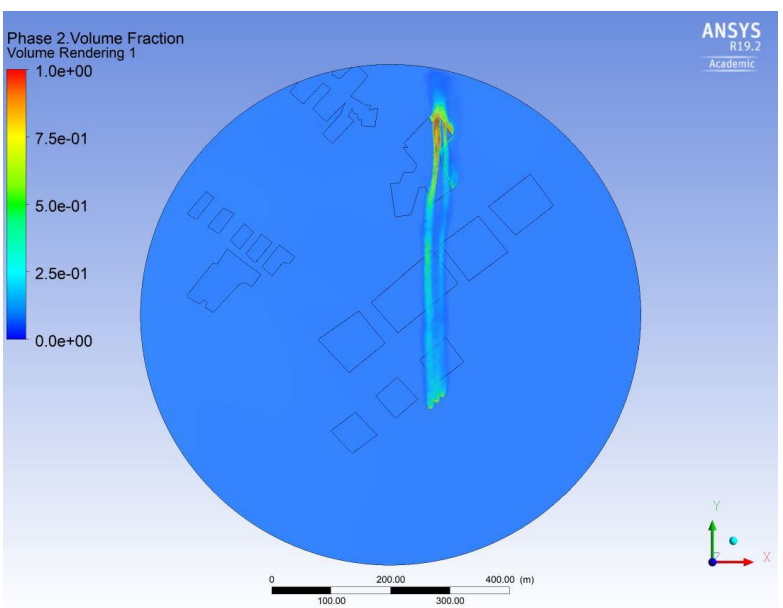

Figure 22: The emission profile under 15 m/s wind conditions (top view).

The emission profile due to the velocity vector of 3.3 m/s wind condition in y direction is shown in Figures 23 and 24.

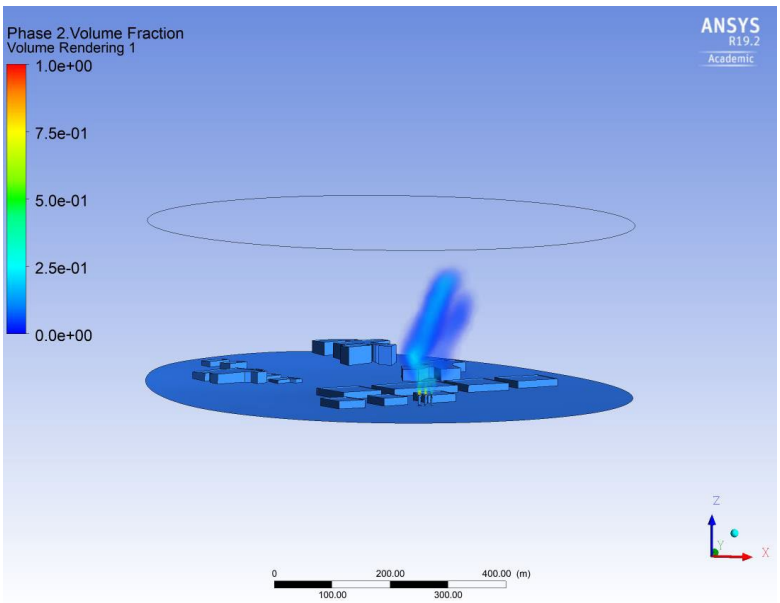

Figure 23: The emission profile under 3.3 m/s wind conditions (side view).

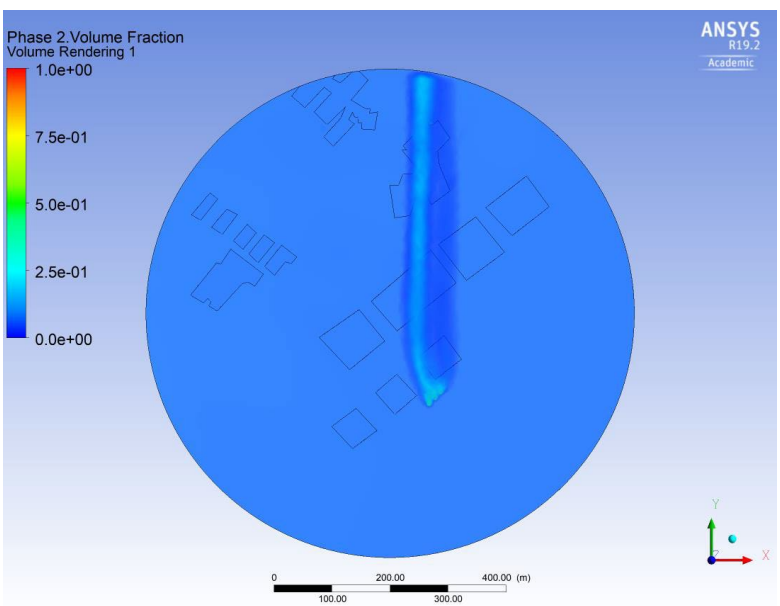

Figure 24: The emission profile under 3.3 m/s wind conditions (top view).

3.4. Chimney Height 5m (ANSYS)

The emission profile due to the velocity vector of 15 m/s wind conditions in y direction is shown in Figures 25 and 26.

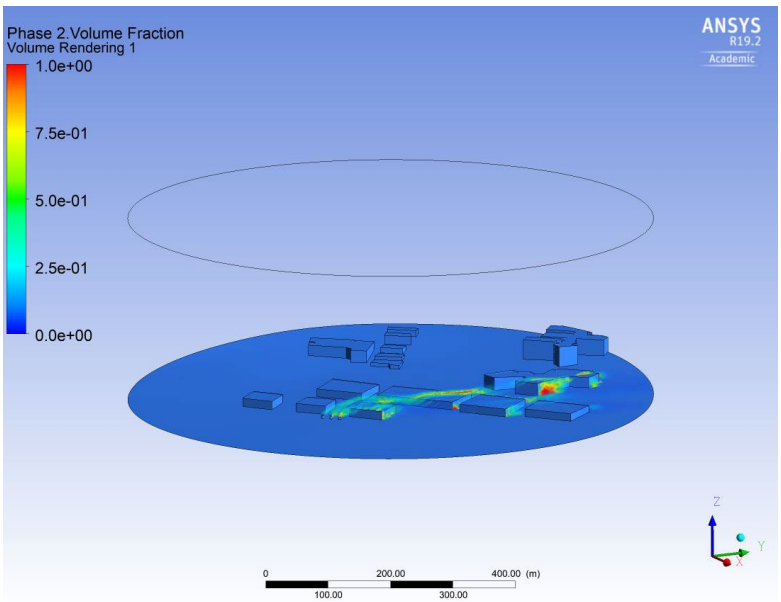

Figure 25: The emission profile under 15 m/s wind conditions (side view).

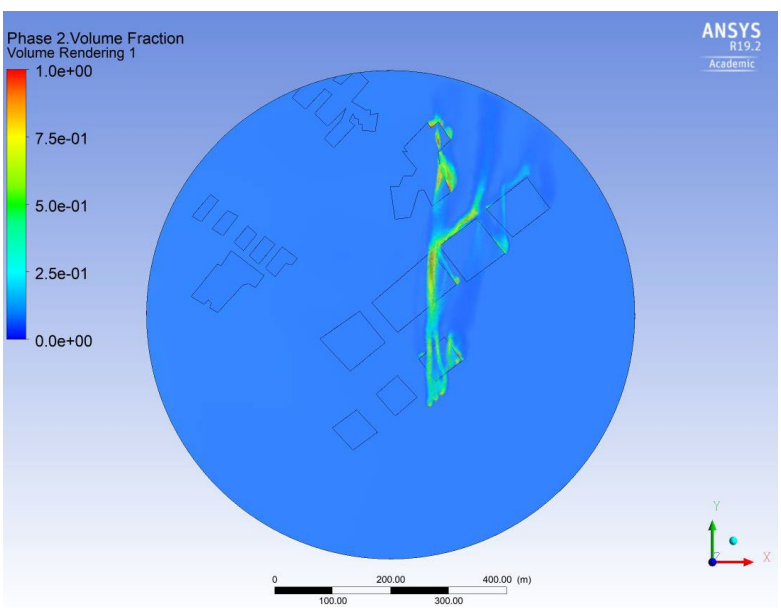

Figure 26: The emission profile under 15 m/s wind conditions (top view).

The emission profile due to the velocity vector of 6.56 m/s wind conditions in negative x-direction and positive y direction with a vector ($\vec{v} = -5\hat{x} + 4.25\hat{y}$) is shown in Figures 27 and 28.

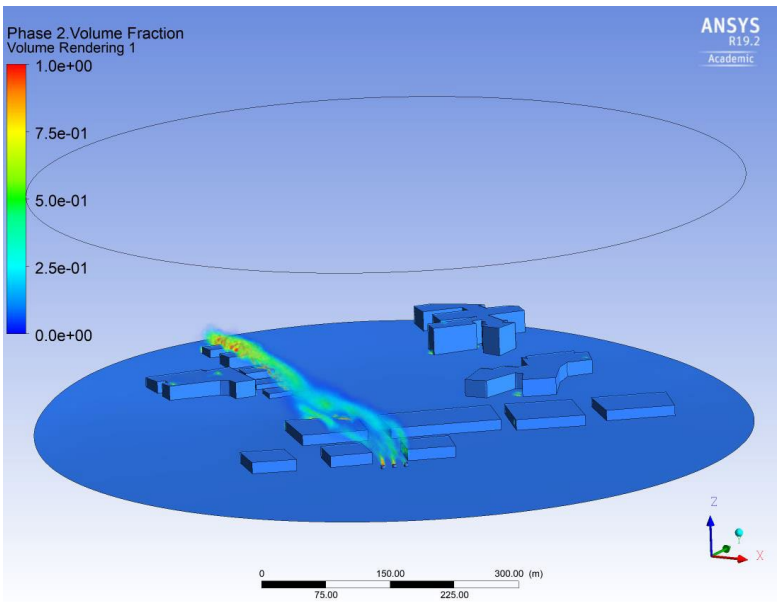

Figure 27: The emission profile under 6.56 m/s wind conditions (side view).

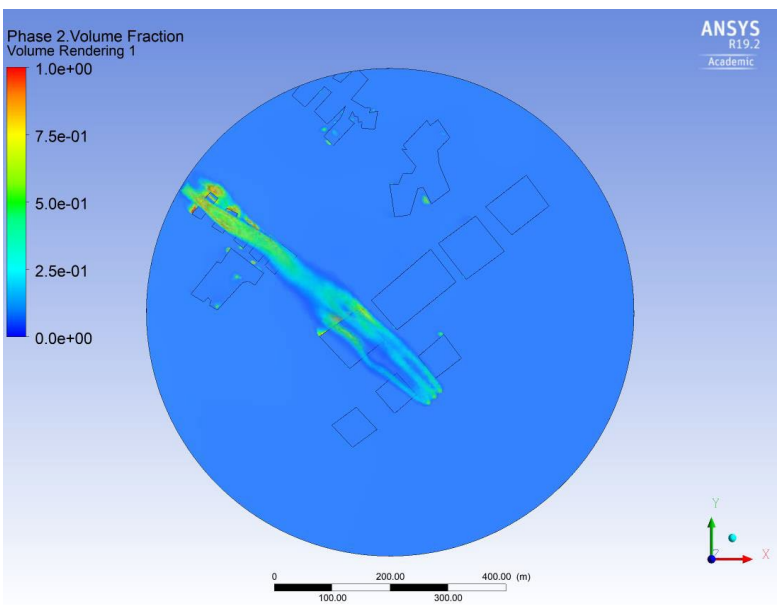

Figure 28: The emission profile under 6.56 m/s wind conditions (top view).

3.5. Chimney Height 30m (OpenFOAM)

The simulations were run using the OpenFOAM CFD software [25] based on the field operation and manipulation (FOAM) C++ class library for continuum mechanics. OpenFOAM uses the finite volume numerical method to integrate the Navier–Stokes equation [26]. The simulated gas mixture is composed of atmospheric air and a trace component that, in this simulation, was identified with carbon dioxide. The trace gas was expelled by the docked vessel through its chimney [27]. In the plume outlet, 40% of the outgoing gas mass corresponded to carbon dioxide. The carbon dioxide fraction at each cell was updated at every time step using the mass conservation equation (Equation (1)). Similar studies were performed by Asier et al. [28-30].

The emission profile due to the velocity vector of 5 m/s wind conditions in y direction is shown in Figures 29 and 30.

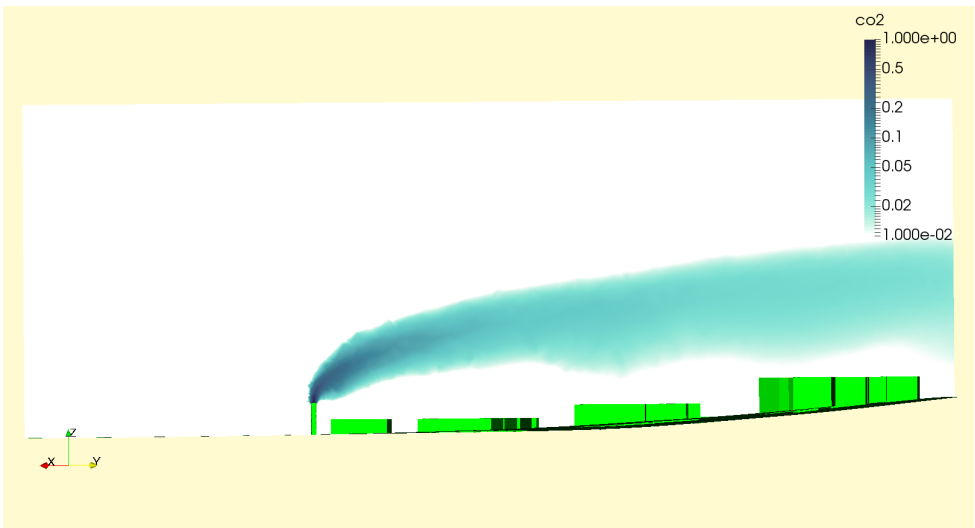

Figure 29: The emission profile under 5 m/s wind conditions (side view).

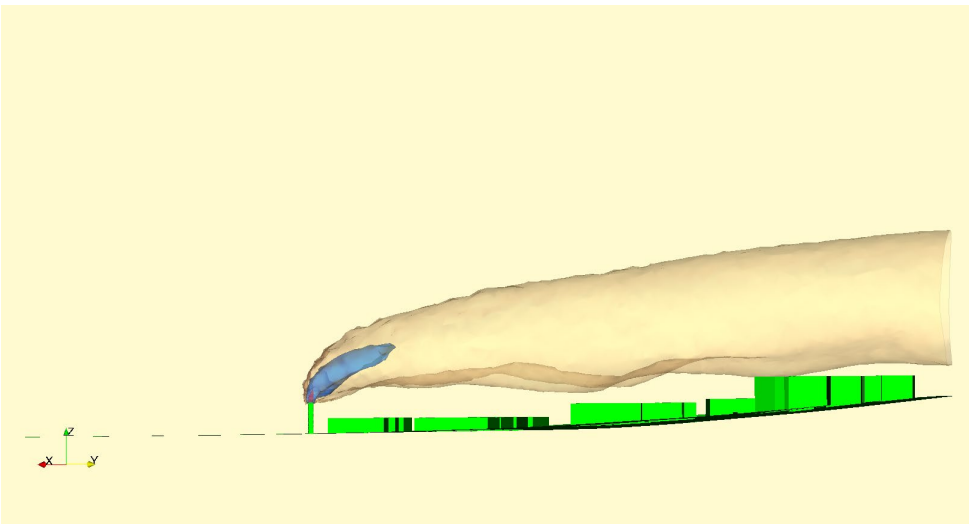

Figure 30: The emission profile under 5 m/s wind conditions (side view).

The emission profile due to the velocity vector of 25.6 m/s wind conditions in negative x-direction and positive y direction with a vector ($\vec{v} = -5.\widehat{4x} + 25\hat{y}$) is shown in Figures 31 and 32.

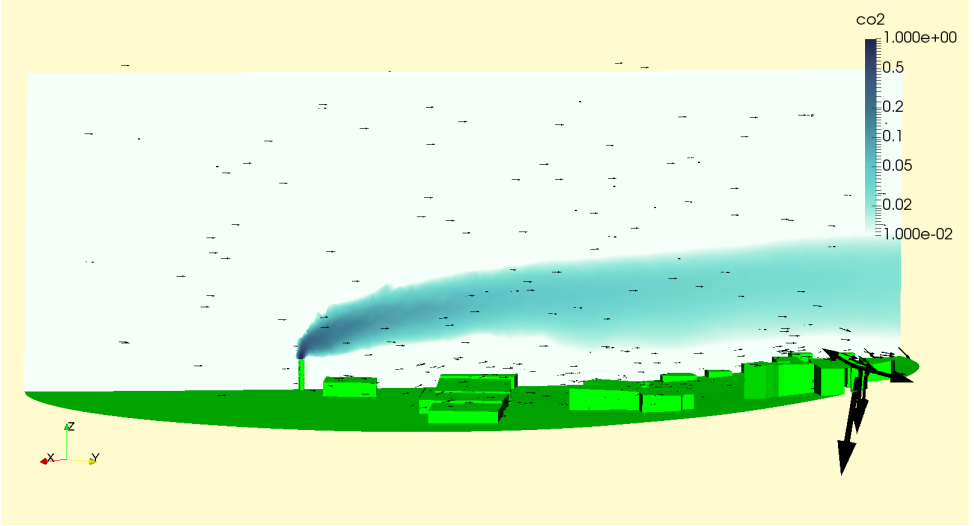

Figure 31: The emission profile under 5 m/s wind conditions (side view).

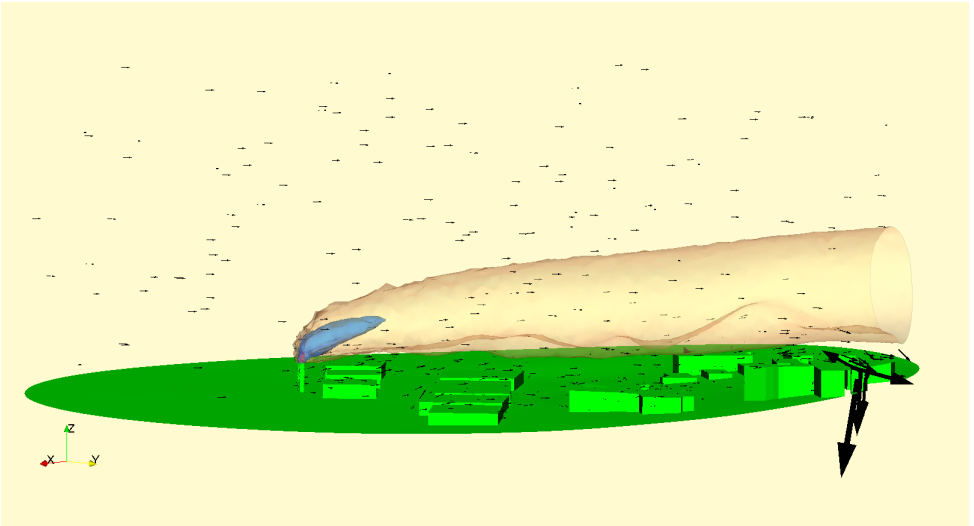

Figure 32: The emission profile under 5 m/s wind conditions (side view).

With a wind strength of 25.58 m/s and a chimney height of 30 m, the plume travel above the buildings without damaging the local environment. The results simulated in OpenFOAM is showing the same qualitatively as visible in ANSYS. The same outcome despite different wind conditions, the plume goes over the buildings. The results from OpenFOAM show a little more diffusion than the results from ANSYS, this might be because of the difference between the software's implementation of the turbulence models. High wind strength effects

within all heights of the pipes. Low wind strength affects when the height of the pipe is low. The lower the pipe is, the less wind strength is required to have a result of carbon dioxide pockets at the local environment. Onshore wind, from east to west, wind from south-east and wind against north affects the emissions.

4. CONCLUSION

From full-scale simulations, it was concluded that lower chimney height and higher wind strengths result in lower plume dispersion, however, the plume stays closer to the terrain. This brings in a concentrated emission pollutants closer to the public areas. Another finding was that greater vessel height results in plumes flowing higher above in the air, not affecting the public areas, and the effect reverses when the vessel's heights are lower. Therefore, it can be assumed that higher vessels are better for public health in terms of the instant release of pollutants for the geographical area. High wind strength and onshore wind make the flow of pollution against the terrain. For the wind strengths affecting the most, the vortex-effect is creating pockets of pollution at the lee side of the buildings. Low wind strength causes the pollution to disperse to air. When the pollution is flowing between buildings in the terrain, pockets of pollution appear. Because of the wind strength and direction, the potential vessel's height of less than 30 meters illustrates this effect. High wind strength combined with a low vessel significantly increase the impact on nearby surroundings.

ACKNOWELDEGEMENT

The publication charges for this article have been funded by a grant from the publication fund of UiT The Arctic University of Norway.

REFERENCES

[1] H. H. Hu, “Computational Fluid Dynamics,” Fluid Mech., pp. 421–472, Jan. 2012-

[2] S. Deshpande, P. Sundsbø, and S. Das, “Ship resistance analysis using CFD simulations in Flow-3D,” Int. J. Multiphys., vol. 14, no. 3, pp. 227–236, Sep. 2020.

[3] G. Boiger, “Euler-LaGrangian model of particle motion and deposition effects in electro-static fields based on openfoam,” Int. J. Multiphys., vol. 10, no. 2, pp. 177–194, 2016.

[4] G. Boiger, M. Mataln, B. Gschaider, and W. Brandstätter, “PART 2: LARGE PARTICLE MODELLING Simulation of particle filtration processes in deformable media,” Int. J. Multiphys., vol. 2, no. 2, pp. 191–206, Jun. 2008.

[5] G. Boiger, M. Boldrini, V. Lienhard, B. Siyahhan, H. Khawaja, and M. Moatamedi, “Multiphysics Eulerian-Lagrangian Electrostatic Particle Spray- And Deposition Model for OpenFOAM® and KaleidoSim® Cloud-Platform,” Int. J. Multiphys., vol. 14, no. 1, pp. 1–16, Mar. 2020.

[6] H. Khawaja, “CFD-DEM Simulation of Minimum Fluidisation Velocity in Two Phase Medium,” Int. J. Multiphys., vol. 5, no. 2, pp. 89–100, 2011.

[7] H. A. Khawaja and M. Moatamedi, “Introduction: discrete element modeling-computational fluid dynamics of fluidized beds,” Multiphysics Model. Fluid-Particulate Syst., pp. 3–22, Jan. 2020.

[8] A. Nordli and H. Khawaja, “Comparison of Explicit Method of Solution for CFD Euler Problems using MATLAB® and FORTRAN 77,” Int. J. Multiphys., vol. 13, no. 2, pp. 203–214, Jun. 2019.

[9] D. Brunner, H. Khawaja, M. Moatamedi, and G. Boiger, "CFD modelling of pressure and shear rate in torsionally vibrating structures using ANSYS CFX and COMSOL Multiphysics," Int. J. Multiphys., vol. 12, no. 4, pp. 349–358, Dec. 2018.

[10] H. A. Khawaja, "CFD-DEM Simulation of Minimum Fluidisation Velocity in Two Phase Medium," Int. J. Multiphys., vol. 5, no. 2, pp. 89–100, Jun. 2011.

[11] Y. Tsuji, T. Kawaguchi, and T. Tanaka, "Discrete particle simulation of two-dimensional fluidized bed," Powder Technol., vol. 77, no. 1, pp. 79–87, 1993.

[12] N. K. Arystanbekova, "Application of Gaussian plume models for air pollution simulation at instantaneous emissions," Math. Comput. Simul., vol. 67, no. 4–5, pp. 451–458, Dec. 2004.

[13] J. C. Weil and R. P. Brower, "An Updated Gaussian Plume Model for Tall Stacks," http://dx.doi.org/10.1080/00022470.1984.10465816, vol. 34, no. 8, pp. 818–827, 2012.

[14] A. E. S. Green, R. P. Singhal, and R. Venkateswar, "Analytic Extensions of the Gaussian Plume Model," http://dx.doi.org/10.1080/00022470.1980.10465108, vol. 30, no. 7, pp. 773–776, 2012.

[15] S. Brusca, F. Famoso, R. Lanzafame, S. Mauro, A. M. C. Garrano, and P. Monforte, "Theoretical and Experimental Study of Gaussian Plume Model in Small Scale System," Energy Procedia, vol. 101, pp. 58–65, Nov. 2016.

[16] J. B. Johnson, "An Introduction to Atmospheric Pollutant Dispersion Modelling," Environ. Sci. Proc. 2022, Vol. 19, Page 18, vol. 19, no. 1, p. 18, Jul. 2022.

[17] L. (Lu) Ting and R. (Rupert) Klein, Viscous vortical flows. Springer-Verlag, 1991.

[18] V. J. Rossow, "On the inviscid rolled-up structure of lift-generated vortices," J. Aircr., vol. 10, no. 11, pp. 647–650, 1973.

[19] I. Tombach, "Observations of Atmospheric Effects on Vortex Wake Behavior," https://doi.org/10.2514/3.60276, vol. 10, no. 11, pp. 641–647, May 2012.

[20] C. V. Okafor, "Finite Element Analysis of Vortex Induced Responses of Multistory Rectangular Building," Eur. J. Eng. Res. Sci., vol. 3, no. 2, p. 35, Feb. 2018.

[21] "Ansys, Engineering Simulation Software." https://www.ansys.com/ (accessed Dec. 12, 2021).

[22] "Earth Versions – Google Earth." https://www.google.com/earth/versions/ (accessed Jun. 18, 2023).

[23] "TCX Converter 2.0 Download (Free) - TCX Converter.exe." https://tcx-converter.software.informer.com/2.0/ (accessed Jun. 18, 2023).

[24] "Ansys Fluent | Fluid Simulation Software." https://www.ansys.com/products/fluids/ansys-fluent (accessed Jun. 18, 2023).

[25] "OpenFOAM." https://www.openfoam.com/ (accessed Jun. 18, 2023).

[26] G. Boiger, "Euler-Lagrangian Model of Particle Motion and Deposition Effects in Electro-Static Fields based on OpenFoam," Int. J. Multiphys., vol. 10, no. 2, pp. 177–194, Jun. 2016, doi: 10.21152/1750-9548.10.2.177.

[27] A. Leyli, S. Jackson, H. Khawaja, and M. Moatamedi, "Modeling of Pressure and Temperature Profiles for the Flow of CO2 through a Restriction," Int. J. Multiphys., vol. 15, no. 2, pp. 235–250, Apr. 2021, doi: 10.21152/1750-9548.15.2.235.

[28] A. Zubiaga, S. Madsen, H. Khawaja, and G. Boiger, "Atmospheric Contamination of Coastal Cities by the Exhaust Emissions of Docked Marine Vessels: The Case of Tromsø," Environ. 2021, Vol. 8, Page 88, vol. 8, no. 9, p. 88, Sep. 2021.

[29] P. Middha and O. R. Hansen, "CFD simulation study to investigate the risk from hydrogen vehicles in tunnels," Int. J. Hydrogen Energy, vol. 34, no. 14, pp. 5875–5886, Jul. 2009, doi: 10.1016/J.IJHYDENE.2009.02.004.

[30] T. Myrvang and H. Khawaja, "Validation of air ventilation in tunnels, using experiments and computational fluid dynamics," Int. J. Multiphys., vol. 12, no. 3, pp. 295–312, Sep. 2018, doi: 10.21152/1750-9548.12.3.295.